Published in final edited form as:
*Curr Biol*. 2004 August 10; 14(15): 1319–1329. doi:10.1016/j.cub.2004.07.052.

# Roundabout 2 Regulates Migration of Sensory Neurons by Signaling In *trans*

**Rachel Kraut** and **Kai Zinn***
Division of Biology 114-96, California Institute of Technology, Pasadena, California 91125

## Summary

**Background—**Roundabout (Robo) receptors and their ligand Slit are important regulators of axon guidance and cell migration. The development of *Drosophila* embryonic sense organs provides a neuronal migration paradigm where the in vivo roles of Slit and Robo can be assayed using genetics.

**Results—**Here we show that Slit-Robo signaling controls migration of *Drosophila* larval sensory neurons that are part of the Chordotonal (Cho) stretch receptor organs. We used live imaging to show that abdominal Cho organs normally migrate ventrally during development, whereas thoracic Cho organs do not. Robo2 overexpression in *cis* (in the sensory neurons) or in *trans* (on neighboring visceral mesoderm) transforms abdominal organs to a thoracic morphology and position by blocking migration, while loss of Slit-Robo signaling produces a reverse transformation in which thoracic organs migrate ectopically. Rescue and tissue-specific knockout experiments indicate that *trans* signaling by Robo2 contributes to the normal positioning of the thoracic Cho organs. The differential positioning of Cho organs between the thorax and abdomen is known to be regulated by Hox genes, and we show that the essential Hox co-factor Homothorax, represses Robo2 expression in the abdominal visceral mesoderm.

**Conclusions—**Our results suggest that segment-specific neuronal migration patterns are directed through a novel signaling complex (the “Slit sandwich”) in which Robo2 on the thoracic visceral mesoderm binds to Slit and presents it to Robo receptors on Cho neurons. The differential positioning of Cho organs between thorax and abdomen may be determined by Hox gene-mediated repression of *robo2*.

## Introduction

The molecular mechanisms that control axon outgrowth and guidance are closely related to those regulating cell migration during development. This has been shown genetically by the fact that several classes of guidance molecules have been characterized for mutant phenotypes that affect both axon pathfinding and cell migration (reviewed in [1–3]). One of the best known of these is the family of Roundabout (Robo) receptors. Robos regulate axon guidance and cell migration in both invertebrate and vertebrate systems ([4–8], see reviews [9, 10]).

The *Drosophila* genome encodes three Robo receptors. The first Robo was discovered in a screen for genes involved in control of axon guidance decisions at the central nervous system (CNS) midline [11]. The phenotypes of *robo* mutant embryos suggested that Robo



*Correspondence: zinnk@its.caltech.edu.

**Supplemental Data**
Three supplemental movies are available online at http://www.current-biology.com/cgi/content/full/14/15/1319/DC1.

mediates repulsion of axonal growth cones in response to signals emanating from the midline. Later work showed that Robo repulsion is triggered by its interactions with Slit, a large secreted protein expressed by midline glia [6, 12–14].

The two other fly Robo family proteins, Robo2 and Robo3, are also Slit receptors that can mediate axonal repulsion from the midline. Robo, Robo2, and Robo3 are expressed in overlapping domains within the longitudinal tracts of the CNS, and the lateral positions of axons relative to the midline are thought to be defined by a combinatorial code of Robo protein expression. It is assumed that Robo and Robo2 have partially redundant activities in mediating axonal repulsion, because *robo, robo2* double mutants have more severe CNS phenotypes than either single mutant. The midline phenotypes of these double mutants resemble those of embryos lacking Slit [15–18].

Slit-Robo signaling has been shown to affect migration of several neuronal types in vertebrate tissue culture experiments. Migrating olfactory neuron precursors in the anterior subventricular zone (SVZa) of the telencephalon can be repelled by Slit secreted from the underlying septum. However, it is unclear whether Slit-Robo interactions control migration in vivo, because *slit* and *robo* knockout mutants do not display migration defects [9, 19]. The phenotypes of loss-of-function (LOF) mutations in the *C. elegans slit* gene show that Slit is a positive regulator of neuronal migration in this system [20].

Slit-Robo signaling can also affect migration and adhesion of nonneural cell types. In *Drosophila*, *slit* and *robo* mutations alter the movement of tracheal precursor cells [21] and affect the selection of epidermal attachment sites by migrating muscle precursors [22]. Mammalian Slit has an inhibitory effect on leukocyte migration toward soluble attractants [3, 23].

In this paper, we describe a novel function of the Robo receptors and of Slit in regulation of migration of sensory neurons and support cells in the *Drosophila* peripheral nervous system (PNS). In the course of a gain-of-function (GOF) screen for genes that affect motor axon morphology [24], we noticed that neuronal overexpression of Robo2 leads to a failure of larval stretch receptors, known as chordotonal (Cho) organs, to assume their proper lateral positions and dendritic orientations within abdominal segments.

To determine the origins of this phenotype, we observed green fluorescent protein (GFP)-expressing nation scent Cho organs in live embryos. We show that the normal lateral positioning of abdominal Cho organ clusters is the result of ventral migration during embryonic development and that overexpression of Robo2 blocks this migration. As a consequence of this blockage, the abdominal Cho organs take on the positioning of thoracic Cho organ clusters, which normally do not migrate and thus remain at a more dorsal position. Elimination of Slit-Robo signaling causes a reverse transformation in which thoracic organs migrate ectopically to the position of abdominal organs. Taken together, these results indicate that Slit and Robo control the segment-specific migration patterns of Cho organs.

Why do abdominal Cho organs migrate in wild-type embryos, while thoracic organs do not? We show that this difference arises because Robo2 is normally expressed on a portion of the visceral mesoderm (VM) that is in contact with nascent thoracic, but not with abdominal, Cho organs. Analysis of LOF and GOF phenotypes suggests that Robo2 on the thoracic VM binds to Slit and presents it to Robo receptors on Cho neurons, thus preventing them from migrating. We also present evidence that homeotic genes may control the segment-specific morphologies of Cho sense organs through repression of Robo2 expression in the abdominal VM.

## Results

### Robo2 Overexpression Transforms Abdominal Chordotonal Organs to a Thoracic Morphology and Position

Each body segment of a *Drosophila* larva contains a stereotyped array of sense organs that arises during embryonic development [25]. A single Cho organ (purple in Figure 1) consists of a neuron with a prominent ex-tended dendrite and several support cells. These include the scolopale, which ensheathes the dendrite, and the cap and ligament cells, which attach the organ to the ectoderm (diagram in Figure 3A). In the abdomen (segments A1–A7), clusters of five parallel chordotonal organs called lCh5s occur in a lateral position, and their dendrites point dorsally and posteriorly (Figures 1B and 2B). In the T2 and T3 thoracic segments, clusters of three parallel chordotonal organs called dCh3s occur in a dorsal position, and their dendrites point ventrally (Figures 1A and 2A). Thoracic dCh3s and the posterior part of the abdominal lCh5 clusters are serially homologous structures, arising from a single precursor cell present in each segment. The precursor of the anterior part of the lCh5 organ appears ~1 hr later in development. Each precursor expresses the same molecular markers, and all Cho organs have the same lineage and morphology [26]. Cho sensory neurons express Robo family proteins, and their ligand Slit is expressed at low levels throughout the mesoderm adjacent to the Cho organs (Figure 4).

We identified an insertion in *robo2 (EP2582)* in our screen of the Rørth collection of GAL4-driven "EP" *P* elements based on peripheral nervous system (PNS) alterations produced when this insertion was crossed to a panneural GAL4 driver [24]. The EP insertion site is about 100 bp upstream of the *robo2* gene's translation start site.

The *C155* driver (an insertion in the *elav* gene) expresses GAL4 in all postmitotic neurons [27, 28]. In *C155/+;EP-robo2/+* (hereafter denoted *elav::robo2*) larvae, abdominal lCh5 organs are transformed so that they resemble thoracic dCh3 organs. The transformed lCh5s are displaced dorsally in the ectoderm. They retain the usual five neurons per cluster, but their dendrites and support cells display a variety of orientations, ranging from the ventral orientation typical of dCh3 organs, through intermediate bent orientations, to orientations similar to those of normal lCh5s (Figures 2D–2G). At 29°C, 44% of abdominal segments in *elav::robo2* animals had partial or complete transformations of Cho organ morphology (Table 1; Figures 2L and 6A).

To examine when transformation takes place, we visualized sensory neurons in *elav::robo2* embryos using monoclonal antibody (mAb) 22C10. These data show that inversion and dorsal displacement of ICh5 organs can be observed as early as stage 14, before the axons of the sensory neurons have reached the CNS (Figure 2J).

Expression of Robo2 protein from the EP line was confirmed by staining *elav::robo2* embryos with anti-Robo2 and 22C10. High levels of Robo2 were detected in the expected panneural pattern, including Cho neurons. Robo2 expression appeared to be primarily at the cell surface (Figure 2C).

Although *elav* drivers confer expression only in the neurons of Cho organs, the entire organ changes position and orientation when it is transformed by *elav*-driven *robo2* expression. This was shown by staining *elav::robo2* embryos with an antibody to Painless, a vanilloid receptor homolog that is expressed only in the cap cells of the Cho organ [29]). The cap cells always follow the orientation of the transformed Cho neurons (Figure 2H).

Transformation of abdominal lCh5 organs (30.5% at 29°C; Table 1, Figure 6A) was also observed when *robo2* expression was driven specifically in the Cho organs by the *atonal*

*(ato)* GAL4 driver [30]. *ato*-GAL4 confers expression in Cho organ precursor cells and later in the Cho neuron and its support cells. It does not drive expression in other sensory neurons. This shows that the transformation observed with the *elav* driver is not induced by neighboring sensory neurons or motor axons that also express *robo2*, but is due to overexpression in Cho neurons.

## Transformation Is Selectively Induced by Robo2

In order to determine if other Robos could also transform lCh5 organs, we crossed UAS-driven Robo family trans-genes to the *elav* driver. To verify that transgene expression driven via the pUAST vector control elements [27] would produce the same effects as endogenous gene overexpression driven by EP elements [27], we first showed that a *UAS-robo2* cDNA transgene also transforms lCh5s (21 % transformation, 41 % total defects at 29°C; Table 1). We then tested equivalent constructs for the other two Robo family members, *robo* and *robo3*, and found that these could not transform at all. However, a *robo* "hyperactive" mutant that contains a tyrosine (Y) to phenylalanine (F) substitution in a regulatory phosphorylation site [31] did transform at a low frequency (6.1%; 8.7% total defects; Table 1, Figure 6A). Thus, our data indicate that transformation is preferentially conferred by Robo2 overexpression but that Robo signaling can also transform to some extent if it is of sufficient strength. Robo2 still transforms when overexpressed in Cho neurons in the absence of Robo, indicating that neuronal expression of Robo is not required (36.4%; Table 1).

Robo contains two cytoplasmic signaling motifs, CC2 and CC3, that are not present in Robo2. These motifs mediate binding to the SH2-SH3 adaptor Dock, as well as to the cytoskeletal modulator Enabled (Ena) and the Abl tyrosine kinase, respectively [31, 32]. To test whether Robo2's ability to transform Cho organs might be due to absence of the CC2 and CC3 motifs, we expressed a Robo transgene that lacks CC2 and CC3 and asked whether it would mimic the activity of *robo2* 31]. This, however, did not transform at all (Table 1).

The Robo2 overexpression phenotype requires interaction with Slit ligand, since removal of one copy of *slit* from *robo2* overexpression embryos attenuated the penetrance of the transformation phenotype by a factor of two (17% in *elav::robo2/+; slit/+* versus 32% in *elav::robo2/+* at 25°C; $p < 0.0005$; Table 1, Figure 6A).

## Transformation Involves Blockage of Abdominal Cho Organ Migration

Cho sense organ precursors (SOPs) in the abdomen and the thorax begin their development at similar dorsoventral positions, although the abdominal SOPs are slightly offset relative to the thoracic SOPs at stage 11 due to curvature of the germband [26]. It has been suggested that the abdominal organs change their positions and morphologies relative to the thoracic organs by migrating ventrally in the ectoderm (or stretching [33]) and rotating so that their dendrites point dorsally [34]. If so, Robo2's conversion of lCh5 organs to a dCh3-like morphology could be caused by inhibition of migration. As no direct evidence for migration has been reported, however, testing this model required us to first determine if lCh5 organs actually do migrate in wild-type animals. This cannot be done by staining fixed embryos for the standard sensory neuron marker 22C10 antigen (Futsch), because the distinctive Cho 22C10 staining pattern does not appear until the organ is in its final position. We thus developed live imaging techniques to directly visualize movement of Cho organs in earlier embryos.

The chordotonal determinant Ato is a transcription factor that is expressed in the chordotonal SOPs at stage 10 [35]. Although expression of endogenous Ato fades by the time the organs differentiate, expression of an EGFP marker [36] driven by the *ato*-Gal4

driver [30] perdures throughout the differentiation process, and GFP is retained by the descendants of the SOPs that form the final organ. We were able to visualize Cho organ precursors in live *ato*-GAL4, UAS-EGFP (*ato*::GFP) embryos. This allowed us to determine whether and when migration of the abdominal organs or their precursors occurs to bring about differential positioning. Figures 3B and 3C show the relationship between GFP expression and neuronal differentiation in fixed *ato*::GFP embryos.

Observation of live *ato*::GFP embryos from stage 12 onward showed that abdominal Cho precursors indeed migrate ventrally relative to their thoracic counterparts. Positional differences can be observed starting at stage 13 and become more pronounced as development progresses through stage 16, when abdominal GFP-positive cells appear to jockey for a more ventral position while thoracic ones remain dorsal (Figures 3L and 3N; see Movie 1 online, which shows a developing *ato*::GFP embryo). The ventral movement of abdominal Chos with respect to the surrounding epidermis was confirmed in a separate experiment, where the changing positions of the GFP-expressing Chos over time were calibrated relative to a stationary spot of DiI injected into the ectoderm. The distance from the DiI spot to the Cho cluster shrinks as development proceeds (Figures 3G–3K).

A projection in the ventral direction from abdominal clusters that is seen at early stage 14 could correspond to one of the nascent neurites that extend from lCh5 neurons. Thoracic clusters also extend projections, but they point dorsally rather than ventrally, consistent with the orientations of the initial segments of the thoracic dCh3 axons in later embryos (Figures 3D and 3E; Movie 1 online).

Having shown that abdominal Cho organs do migrate ventrally, we then simultaneously expressed Robo2 and EGFP from the *ato*-GAL4 driver and used live imaging to visualize Cho organs in these embryos. Since *ato::robo2* causes lCh5 transformation with a penetrance of ~30% (Table 1), we expected that one or two abdominal Cho clusters on each side of an embryo might behave differently from their counterparts in other segments. We did in fact observe abdominal clusters that failed to migrate in these embryos (Figures 3M and 3O; Movies 2A and 2B online), suggesting that Robo2 had blocked their migration. Some of these “stalled” abdominal clusters extended projections dorsally (Figure 3F; Movies 2A and 2B).

## Loss of Robo Signaling Produces Transformation of Thoracic Chordotonal Organs to an Abdominal Morphology and Position

To determine the relevance of our Robo2 overexpression findings to wild-type development, we examined *slit, robo,* and *robo2* LOF mutants for Cho morphology defects. The overexpression results described above suggest that the dorsal positioning of the thoracic dCh3 Cho organs in wild-type animals is due to inhibition of their migration through Slit-Robo signaling. If so, then the “default” dCh3 organ phenotype in the absence of Slit or of Robos should be migration and rotation to acquire an lCh5-like morphology.

Loss of zygotic *slit* function, which would be expected to greatly reduce signaling through all Robo receptors, does in fact produce transformation of dCh3 organs to an abdominal morphology (Figures 4D and 6B, Table 2; see also [37]). All three Robos can bind to Slit, and generation of a *slit*-like CNS phenotype requires loss of both Robo and Robo2 [16, 17]. We found this to be the case for Cho organ migration as well. Single LOF mutations in *robo* or *robo2* produce no dCh3 phenotypes, while loss of both Robos causes thoracic-to-abdominal morphology transformations identical to those seen in *slit* mutants (Figures 4C and 6B, Table 2).

These results indicate that binding of Slit to Robo and Robo2 on thoracic Cho organs produces signals that prevent their migration in wild-type animals. This conclusion, however, raises the question as to why the levels of Slit-Robo signaling should normally be lower in the abdominal organs that do migrate. To address this, we examined Slit, Robo, and Robo2 expression in the periphery of wild-type embryos during the period of Cho organ migration. Slit is expressed in the mesoderm at a uniform level along the body axis (Figures 4E and 4F). Robo2 is expressed in ectodermal domains between the Cho precursors during stages 12–14 (Figures 5A, 5B, and 5E; Movie 3 online), and Robo and Robo2 are both expressed in Cho neurons at later stages (Figures 4G and 4H). There are no differences in Robo or Robo2 expression levels or localization between the abdomen and the thorax in the Cho neurons or ectoderm. We could not detect any Robo3 in Cho neurons, but a recent paper reported that it is expressed at low levels by these cells [38].

Since we did not find any differences in Robo, Robo2, or Slit expression in thoracic versus abdominal Cho organs or ectoderm that could explain the different migratory behaviors of the two populations, we searched elsewhere for segment-specific domains of Robo family protein expression. We found that at the time of Cho organ migration, Robo2 is expressed at high levels in a patch of VM in the T2 and T3 segments but is not detected in abdominal VM (Figures 5A, 5B, and 5E; Movie 3 online). Three-dimensional reconstructions of confocal z-series from embryos double-stained for Robo2 and 22C10 (Figure 5B; Movie 3) show that the thoracic Robo2-expressing portion of the VM directly contacts the thoracic Cho organ precursors that do not migrate (schematically illustrated in Figure 5B'). A rotating rendering of a Robo2-and 22C10-stained embryo shows this apposition graphically (Movie 3).

## Mesodermal Robo2 Regulates Neuronal Migration In *trans*

If the thoracic expression of Robo2 in the VM were the source of signaling to the nonmigrating thoracic Cho organs, one would predict that driving Robo2 in the abdominal VM would likewise inhibit migration in the overlying abdominal Cho organs. We tested this using a GAL4 driver, *48Y*, which confers expression in the entire VM and in the midgut endoderm (Figures 5C and 5D) [39]. Three-dimensional reconstruction of Robo2/22C10-stained *48Y::robo2* embryos showed that the ec-topic Robo2 expression domain in the abdominal VM now contacts the abdominal Cho organs at the time of their migration (stage 14; Figure 5D). When examined at stage 16, *48Y::robo2* embryos showed transformation of 17% of abdominal lCh5 organs to dCh3-like positions and morphologies (Figures 5H and 6A; Table 1). As with the neuronal *(elav)* and Cho organ (*ato*) drivers, intermediate lCh5 phenotypes were also observed (Figure 5H). These results show that Robo2 can prevent migration and thus induce transformation when it is expressed either in *cis* or in *trans* to Robo receptors in Cho neurons (i.e., in Cho neurons themselves [*cis*] or in the apposed VM [*trans*])

Interestingly, abdominal-to-thoracic Cho organ transformations very similar to those produced by Robo2 overexpression are also seen in embryos bearing mutations in the homeotic gene *homothorax (hth)* (Figure 5G) [34, 40, 41]. We wondered whether this transformation could be caused by alterations in Robo2 expression, so we examined *hth* mutant embryos by staining for Robo2. In these embryos, Robo2 is now ectopically expressed in the abdominal VM, adjacent to abdominal Chos (Figure 5F). Thus, abdominal Cho organs in $hth^{-}$ embryos may be transformed by virtue of their apposition to ec-topic abdominal Robo2. Our results thus suggest that repression of Robo2 expression in abdominal VM is a mechanism through which homeotic genes regulate segment-specific Cho organ positioning.

### Knockout and Rescue Evidence for Robo2 Signaling In *trans*

The results described above show that loss of Robo signaling produces ectopic ventral migration and transformation of thoracic Cho organs to an abdominal morphology. Robo and Robo2 are expressed in Cho organs in all segments (Figure 4). However, Robo2 is localized to the VM underlying thoracic Cho organs, suggesting that it may signal in *trans* to prevent their migration. Consistent with this, ectopic expression of Robo2 in the abdominal VM blocks ventral migration of abdominal Cho organs (Figure 5).

To show that Robo2 expression in the VM is required for blockage of thoracic Cho organ migration in wild-type embryos, we used the Commissureless (Comm) protein to knock out Robo family proteins in a tissue-specific manner. Comm causes diversion of Robos to a degradative pathway and prevents them from signaling [42]. When we drove endogenous Comm expression in the VM (via an EP element) with *48Y-GAL4,* we observed that a substantial fraction (~20%) of thoracic Cho organs shifted to a lateral position and orientation characteristic of abdominal organs (Table 2, Figure 6B). These results indicate that eliminating all Robo family signaling from the VM can allow thoracic Cho organs to migrate ventrally.

To further evaluate how Robo2 confers differences in migration behavior between the thoracic and abdominal Cho organs, we assessed rescue of the *robo, robo2* Cho organ migration phenotype by restoring Robo2 expression in the VM (via the *48Y-GAL4* driver) or in the Cho neurons (via the *elav-GAL4* driver). We found that ectopic thoracic Cho organ migration is reduced from 35.9% to 16% ($p = 0.001$) by high-level Robo2 expression in the VM (*trans* rescue; Table 2, Figure 6B). These results show that mesodermal Robo2 provided by a transgene can signal to thoracic Cho neurons and prevent their migration.

When Robo2 is overexpressed in Cho neurons in a *robo, robo2* mutant background (*cis* rescue), ectopic migration of thoracic Chos is also reduced, to 11.2% ($p < 0.0005$; Table 2, Figure 6B). This rescue indicates that high-level expression of Robo2 in thoracic Cho neurons of *robo, robo2* mutants (i.e., in the absence of Robo2 expression in the thoracic VM) causes them to respond like abdominal Cho organs overexpressing Robo2 in otherwise wild-type embryos: that is, they fail to migrate ventrally even though they are not apposed to Robo2-expressing VM cells.

Finally, we addressed the mechanisms involved in *trans* Robo2 signaling by expressing a version of Robo2 lacking the cytoplasmic domain (Robo2Δcyt; a kind gift of J. Simpson) in the VM. If Robo2 on the thoracic VM functions through presentation of bound Slit to Robos on the Cho neurons, one might expect that intracellular signaling downstream of Robo2 would not be absolutely necessary to send the signal from the VM. Robo2Δcyt should bind to Slit but be unable to activate downstream signaling. In fact, we found that VM Robo2Δcyt expression can produce a low frequency of abdominal-to-thoracic transformations like those conferred by overexpression of wild-type Robo2 (5.4%; 14.2% total abdominal Cho defects; Table 1, Figure 6A). (Note that Robo2Δcyt might also function as a dominant-negative by heterodimerizing with signaling-competent Robo family members, and this complicates the interpretation of its GOF phenotype. Consistent with this idea, Ro-bo2Δcyt expression in the VM also generates reverse [thoracic-to-abdominal] transformations [9%; Table 1]).

## Discussion

We have demonstrated a novel role for Slit-Robo signaling in regulating segment-specific migration of stretch-sensing Cho organs in the *Drosophila* larval PNS. Vertebrate tissue culture experiments have indicated that Slits and Robos affect neuronal migration ([43–47],

reviewed in Wong et al. [9]). Our results, however, demonstrate directly that migration of sensory neurons in vivo is controlled by the level of activity of Robo receptors. As a consequence of Slit-Robo signaling, thoracic dCh3 Cho organ clusters do not migrate during embryonic development and thus remain in dorsal positions. Abdominal lCh5 organ clusters receive a lower level of Slit-Robo signal and therefore migrate ventrally to take up lateral positions.

In our experiments, we initially observed that Robo2 overexpression in Cho neurons transforms abdominal Cho organs to a thoracic morphology and position (Figures 2 and 6A, Table 1). To understand how this transformation arises, we examined Cho organ development in wild-type embryos. It had been proposed, but never demonstrated, that the abdominal organs migrate ventrally during development, while thoracic organs fail to migrate and thus remain in a more dorsal position [34, 48]). We observed migrating GFP-expressing Cho organs in living animals and showed that migration does in fact occur in wild-type embryos. This migration is impeded when Robo2 is overexpressed (Figure 3; Movies 1 and 2 online).

By analyzing LOF mutants, we then showed that Slit-Robo signaling is relevant to the control of segment-specific Cho organ migration in wild-type animals. In *slit* mutants, a phenotype is observed that is the opposite of the Robo2 overexpression phenotype: thoracic dCh3 organs abnormally migrate ventrally to take up the positions and orientations characteristic of abdominal lCh5 organs. Robo receptors are also required for this process. Robo and Robo2 have partially redundant roles, however, because ectopic migration is seen in *robo, robo2* double mutants, but not in single mutants (Figures 4 and 6B; Table 2).

The overexpression and LOF phenotypes suggest that Slit-Robo signaling is normally stronger in the thoracic Cho organs than in their abdominal counterparts and that this increased signaling blocks ventral migration of the thoracic organs. Overexpression of Robo2 in abdominal Cho organs may prevent their migration by increasing Slit-Robo signaling to levels equal to or above that normally experienced by thoracic Cho organs.

What accounts for the differences in Slit-Robo signaling between thoracic and abdominal segments in wild-type embryos? There are no obvious differences in Robo family protein expression between thoracic and abdominal Cho neurons, and Slit is expressed uniformly along the longitudinal axis of the mesoderm (Figure 4). However, Robo2 is expressed in the thoracic part of the visceral mesoderm (VM), but not in abdominal VM (Figure 5; Movie 3 online). When we ectopically expressed Robo2 in abdominal VM using a GAL4 driver, abdominal-to-thoracic transformations of Cho organs were observed. These transformations appear identical to those seen when Robo2 is overexpressed in the Cho organs themselves (Figures 5 and 6A; Table 1). This result demonstrates that mesodermal Robo2 can signal in *trans* to block migration of Cho neurons.

We then performed tissue-specific knockout and rescue experiments to show that *trans* Robo2 signaling from the VM contributes to positioning of thoracic Cho organs in wild-type animals. Elimination of Robo family proteins from the VM of wild-type embryos by mesoderm-mal expression of Comm, a protein that causes internalization and downregulation of Robos [42], produces thoracic Cho organ ectopic migration phenotypes. We also found that when Robo2 is restored to the VM in a *robo, robo2* double mutant, the frequency of ectopic migration of thoracic Cho organs is reduced (Figure 6B, Table 2).

Our results are consistent with a novel model for Robo signaling in thoracic Cho organs that we call a “Slit sandwich” (Figure 7). In T2 and T3, Robo2 on the surfaces of VM cells binds to Slit, increasing its effective concentration or changing its conformation. This Robo2 bound Slit then interacts with Robo and Robo2 on the thoracic Cho neurons, and

downstream signaling within these neurons prevents the ventral migration of the thoracic Cho organs. In abdominal Cho neurons, the strength of the signal produced by Robo and Robo2 binding to the mesodermal Slit is insufficient to prevent migration. In this model, Robo2 is acting both in *cis* (in the Cho neurons) and in *trans* (on the VM) to influence migration. We suggest that its action in *trans* is due primarily to binding and presentation of Slit to Cho neurons by the Robo2 extracellular domain on VM cells. This model is formally analogous to that proposed for Netrin-Frazzled signaling at the CNS midline, where Frazzled receptor on axons rearranges the distribution of Netrin ligand released from midline glia [49].

There are several possible models for how Robo family protein signaling mediated by the Slit sandwich influences migration. First, Robo signaling in thoracic Cho neurons might neutralize the responses of the organ to unknown ventral attractants. This would be analogous to the blockage of chemokine attraction by Slit in leukocytes [23]. Second, Robo signaling might regulate adhesion of the organ to an epidermal substrate during migration. It is unlikely that such adhesion occurs through direct Robo-Robo interactions, as has been proposed for stimulation of neurite outgrowth in tissue culture [49], since the actions of Robos in our system require Slit. In other studies, however, it has been shown that Slit-Robo signaling can decrease N-cadherin-dependent adhesion [50]. Perhaps the ventral migration of abdominal Cho organs depends on adhesion of Cho neurons to the epidermis, and increased Slit-Robo signaling negatively influences migration by reducing adherence.

Only Robo2 can block migration of abdominal Cho organs through overexpression, both in *cis* (in the Cho neurons) and in *trans* (in the VM). Wild-type Robo and Robo3 do not affect Cho organs when they are overexpressed in either pattern. These results suggest that the excess Robo signal that is required to block migration is most efficiently produced by Robo2. Differences in *cis* signaling in Cho neurons could be explained by the divergent sequences of cytoplasmic domains among the Robo family members. Robo2 acts in lateral CNS tracts, where levels of midline-produced Slit should be low [15, 18]. It may thus have a greater ability to block migration in *trans* because it is more effective in presenting Slit to Robos on the Cho neurons.

The phenotypes described here are not completely penetrant: more than half of the thoracic Cho organs remain at their normal positions even in *slit* or *robo, robo2* null mutants. This could be due to maternally contributed Slit or Robos or to another signaling system that regulates migration. Our observation that driving Comm expression in the VM can produce ectopic migration phenotypes while removal of zygotic Robo2 does not could also be explained by Comm downregulation of maternally contributed Robos. Finally, maternal Robos and/or zygotic Robo3 might account for the ability of thoracic Cho neurons in *robo, robo2* embryos to respond to restoration of Robo2 on the VM (Figure 6B, Table 2). Alternatively, as suggested by a recent analysis of *slit* and *robo* phenotypes in the mouse [51], other neuronal Slit receptors might exist.

## Control of Chordotonal Organ Migration by Homeotic Genes

Mutations in the genes encoding the homeodomain proteins Hth, Extradenticle (Exd), and Abd-A produce abdominal Cho organ phenotypes that resemble those conferred through Robo2 overexpression [34, 40, 41] (Figure 5). Hth and Exd form complexes with Hox proteins, and these can both activate and repress gene expression [40, 52–54]. We examined *hth* mutant embryos and discovered that they now express Robo2 in the abdominal VM as well as in the thorax (Figure 5). This suggests that Hox protein complexes regulate segment-specific Cho organ morphology partly by repression of Robo2 in the abdominal VM. Interestingly, there is a consensus Hth/Exd/Hox binding site within the *robo2* gene (R.

Mann, personal communication), so *robo2* might be a direct target of transcriptional control by Hox complexes.

## Conclusions

The Robo receptors and their ligand Slit are known primarily for their roles in axon guidance in a variety of systems. We have shown that Slit and the Robos also control neuronal migration in vivo, using *Drosophila* peripheral sensory organs as a model system. Our work shows that stretch-sensing Cho organs in abdominal segments migrate ventrally during development, while thoracic Cho organs remain stationary, and that migration of the abdominal Cho organs can be blocked by elevating Slit-Robo signaling. Removal of Slit or of Robos causes thoracic Cho organs to migrate ventrally like their abdominal counterparts. The differential migration of thoracic versus abdominal Cho organs is programmed by localization of Robo2 to a patch of thoracic mesoderm that contacts the Cho neurons. We propose that mesodermal Robo2 presents Slit to Robo family receptors on the Cho organs and that formation of this complex (the Slit sandwich) sends a signal that prevents the thoracic organs from migrating. Control of mesodermal Robo2 expression may be a mechanism by which homeotic genes control the segment-specific morphologies of peripheral sensory organs.

## Experimental Procedures

### Fly Stocks and Overexpression Experiments

EP(2)2582 is an EP line from the collection of P. Rørth. The *C155* driver, a GAL4 transgene inserted in the endogenous *elav* locus [28], was used either alone or combined with UAS-2EGFP, which contains two tandem copies of EGFP separated by an IRES [36] to drive expression of *EP(2)2582* and other UAS lines (below) in Cho neurons. *Atonal-GAL4* 30] combined with UAS-2EGFP (ato::EGFP) was used to drive EGFP expression in Cho organs from stage 12 onward for the time-lapse recordings of wild-type Cho development. For time-lapse recordings of Robo2-overexpressing Chos, homozygous *ato*::EGFP females were crossed with homozygous *EP(2)2582; UAS-2EGFP* males. The following *robo* mutant fly stocks were obtained from J. Simpson and C. Goodman: null mutants $robo^{Z2130}$; $robo2^{ex135}$; $robo3^{1}$; double mutant $robo^{GA285}$, $robo2^{ex135}$; $slit^{2}$. The *homothorax P* allele $hth^{05745}$ 54] is a hypomorph and was obtained from the Bloomington Stock Center. Balancers were detected using *CyO, P[wingless-lacZ]* or *CyO, P[armadillo-GFP]* or *TM3, P[fushi-tarazu-lacZ].* Flies homozygous for the mesodermal driver *48Y-GAL4* were obtained from R. Mann [39] and were crossed to homozygous *EP(2)2582* and to UAS lines. UAS-robo [5], UAS-roboY→F [31], UAS-robo2$^{myc}$ [16], UAS-robo3$^{myc}$ [15], UAS-roboΔCC2, CC3 [31], and UAS-roboΔAcyto$^{myc}$ were obtained from Greg Bashaw and Julie Simpson. The UAS-robo2Δcyto$^{myc}$ construct contains the endogenous amino acid sequence KRKHM immediately C-terminal to the transmembrane domain, followed by a myc-tag. *cis* (Cho neuronal) rescue of the *robo, robo2* thoracic migration phenotype was done by crossing *elav-gal4;* $robo^{GA285}$, $robo2^{ex135}$/*CyLacZ* with $robo^{GA285}$, $robo2^{ex135}$/*CyOLacZ;* *UAS-*$robo2^{myc}$. Trans (VM) rescue of the *robo, robo2* thoracic migration phenotype was done by creating the triple recombinant chromosome $robo^{z2130}$, $robo2^{ex135}$, *48Y* and crossing this to $robo^{GA285}$, $robo2^{ex135}$*/CyOLacZ; UAS-*$robo2^{myc}$. EP-commissureless was obtained from a collection of EP lines generated by Q. Sun and K.Z. (unpublished results).

### Antibodies and Imaging

Rabbit anti-GFP (Clontech) was used at a concentration of 1:500. Affinity-purified rabbit anti-Robo2 (a generous gift of S. Rajagopalan) was used at a concentration of 1:500. mAbs 13C9 and 14C9 against Robo and Robo3, respectively [15], were used at a concentration of

1:10 and were from the Goodman lab. Affinity-purified rabbit anti-Painless [29], used to label Cho cap cells, was a kind gift of D. Tracey. mAb 22C10 [55] was used for assessment of Cho transformation in all experiments. mAbs C555.6 (anti-Slit) and 9E10 (anti-Myc epitope) were obtained from the University of Iowa Developmental Studies Hybridoma Bank and used at a concentration of 1:10.

Time-lapse imaging of live embryos was done on an inverted Zeiss LSM5 Pascal with a 20×/0.7 n.a. air lens. Live embryos were collected at 29°C to maximize UAS-transgene expression, dechorionated in 50% bleach, washed in 0.01 % TritonX-100 and water, and spread onto a clear agar plate. GFP-positive embryos at stage 12 were selected and immersed into a well of molten 1 % low-melting-point agarose in Ringer's solution on a 35 mm Petri dish with a hole cut in the center and a 0.1 mm coverslip glued to the underside (Mat-Tek). Embryos in agarose were covered with a drop of 70S halocarbon oil, and the Petri dish was kept covered during imaging to prevent dessication. For DiI labeling (Figures 3G–3K), embryos were placed on a coverslip under halocarbon oil and injected with DiI, according to the method of Schmid et al. [56]. Parallel transmitted light and fluorescent light images were captured as a 512 × 512 pixel z-series every 1–2 min from late stage 12 to stage 16 (~3.5 hr). z-series were projected with Zeiss software, processed in Adobe Photoshop6 (Adobe Systems, Inc.), and imported as a series of tif files into Quicktime6 Pro (Apple Computer, Inc).

Three-dimensional volume renderings of Robo2 expression were done with Amira (Template Graphics Software, Inc., San Diego, CA). Confocal z-stacks were taken with a Zeiss LSM510 Meta confocal microscope, using a 40×/1.3 na oil lens. For wild-type the voxel size was 0.41 × 0.41 × 0.41 μm, and for VM::robo2 the voxel size was 0.64 × 0.64 × 0.89 μm. Conventional projections were done with Zeiss LSM510 software.

## Acknowledgments

We are very grateful to Aloisia Schmid for doing the DiI injections in Figure 3. We thank the members of the Zinn group, Peter Kolodziej, Richard Mann, Julie Simpson, and Greg Bashaw for helpful discussions; Julie Simpson, Greg Bashaw, Richard Mann, Bassem Hassan, Hugo Bellen, and Marc Halfon for constructs and fly stocks; Srikanth Rajagopalan, Sunita Kramer, and Dan Tracey for antibodies; and Cyrus Papan and Dan Darcy for their expert help with imaging. Imaging work was performed at the Caltech Biological Imaging Facility. This work was supported by an NIH RO1 grant, NS28182, to K.Z. R.K. was supported by an NIH postdoctoral fellowship.

## References

1. Dickson BJ. Molecular mechanisms of axon guidance. Science. 2002; 298:1959–1964. [PubMed: 12471249]
2. Montell DJ. The genetics of cell migration in *Drosophila melanogaster* and *Caenorhabditis elegans* development. Development. 1999; 126:3035–3046. [PubMed: 10375496]
3. Rao Y, Wong K, Ward M, Jurgensen C, Wu JY. Neuronal migration and molecular conservation with leukocyte chemotaxis. Genes Dev. 2002; 16:2973–2984. [PubMed: 12464628]
4. Zallen JA, Yi BA, Bargmann CI. The conserved immunoglobulin superfamily member SAX-3/Robo directs multiple aspects of axon guidance in C. *elegans*. Cell. 1998; 92:217–227. [PubMed: 9458046]
5. Kidd T, Brose K, Mitchell KJ, Fetter RD, Tessier-Lavigne M, Goodman CS, Tear G. Roundabout controls axon crossing of the CNS midline and defines a novel subfamily of evolutionarily conserved guidance receptors. Cell. 1998; 92:205–215. [PubMed: 9458045]
6. Li HS, Chen JH, Wu W, Fagaly T, Zhou L, Yuan W, Dupuis S, Jiang ZH, Nash W, Gick C, et al. Vertebrate slit, a secreted ligand for the transmembrane protein roundabout, is a repellent for olfactory bulb axons. Cell. 1999; 96:807–818. [PubMed: 10102269]
7. Hutson LD, Chien CB. Pathfinding and error correction by retinal axons: the role of astray/robo2. Neuron. 2002; 33:205–217. [PubMed: 11804569]

8. Erskine L, Williams SE, Brose K, Kidd T, Rachel RA, Goodman CS, Tessier-Lavigne M, Mason CA. Retinal ganglion cell axon guidance in the mouse optic chiasm: expression and function of robos and slits. J. Neurosci. 2000; 20:4975–4982. [PubMed: 10864955]
9. Wong K, Park HT, Wu JY, Rao Y. Slit proteins: molecular guidance cues for cells ranging from neurons to leukocytes. Curr. Opin. Genet. Dev. 2002; 12:583–591. [PubMed: 12200164]
10. Rusch J, Van Vactor D. New Roundabouts send axons into the Fas lane. Neuron. 2000; 28:637–640. [PubMed: 11163255]
11. Seeger M, Tear G, Ferres-Marco D, Goodman CS. Mutations affecting growth cone guidance in *Drosophila:* genes necessary for guidance toward or away from the midline. Neuron. 1993; 10:409–426. [PubMed: 8461134]
12. Brose K, Bland KS, Wang KH, Arnott D, Henzel W, Goodman CS, Tessier-Lavigne M, Kidd T. Slit proteins bind Robo receptors and have an evolutionarily conserved role in repulsive axon guidance. Cell. 1999; 96:795–806. [PubMed: 10102268]
13. Kidd T, Bland KS, Goodman CS. Slit is the midline repellent for the robo receptor in *Drosophila*. Cell. 1999; 96:785–794. [PubMed: 10102267]
14. Battye R, Stevens A, Jacobs JR. Axon repulsion from the midline of the *Drosophila* CNS requires slit function. Development. 1999; 126:2475–2481. [PubMed: 10226006]
15. Simpson JH, Bland KS, Fetter RD, Goodman CS. Short-range and long-range guidance by Slit and its Robo receptors: a combinatorial code of Robo receptors controls lateral position. Cell. 2000; 103:1019–1032. [PubMed: 11163179]
16. Simpson JH, Kidd T, Bland KS, Goodman CS. Short-range and long-range guidance by slit and its Robo receptors. Robo and Robo2 play distinct roles in midline guidance. Neuron. 2000; 28:753–766. [PubMed: 11163264]
17. Rajagopalan S, Nicolas E, Vivancos V, Berger J, Dickson BJ. Crossing the midline: roles and regulation of Robo receptors. Neuron. 2000; 28:767–777. [PubMed: 11163265]
18. Rajagopalan S, Vivancos V, Nicolas E, Dickson BJ. Selecting a longitudinal pathway: Robo receptors specify the lateral position of axons in the *Drosophila* CNS. Cell. 2000; 103:1033–1045. [PubMed: 11163180]
19. Patel K, Nash JA, Itoh A, Liu Z, Sundaresan V, Pini A. Slit proteins are not dominant chemorepellents for olfactory tract and spinal motor axons. Development. 2001; 128:5031–5037. [PubMed: 11748139]
20. Hao JC, Yu TW, Fujisawa K, Culotti JG, Gengyo-Ando K, Mitani S, Moulder G, Barstead R, Tessier-Lavigne M, Bargmann CI. *C. elegans* slit acts in midline, dorsal-ventral, and anterior-posterior guidance via the SAX-3/Robo receptor. Neuron. 2001; 32:25–38. [PubMed: 11604136]
21. Englund C, Steneberg P, Falileeva L, Xylourgidis N, Samakovlis C. Attractive and repulsive functions of Slit are mediated by different receptors in the *Drosophila* trachea. Development. 2002; 129:4941–4951. [PubMed: 12397103]
22. Kramer SG, Kidd T, Simpson JH, Goodman CS. Switching repulsion to attraction: changing responses to slit during transition in mesoderm migration. Science. 2001; 292:737–740. [PubMed: 11326102]
23. Wu JY, Feng L, Park HT, Havlioglu N, Wen L, Tang H, Bacon KB, Jiang Z, Zhang X, Rao Y. The neuronal repellent Slit inhibits leukocyte chemotaxis induced by chemotactic factors. Nature. 2001; 410:948–952. [PubMed: 11309622]
24. Kraut R, Menon K, Zinn K. A gain-of-function screen for genes controlling motor axon guidance and synapto-genesis in *Drosophila*. Curr. Biol. 2001; 11:417–430. [PubMed: 11301252]
25. Campos-Ortega, JA.; Hartenstein, V. The Embryonic Development of *Drosophila melanogaster*. 2nd edition. Berlin: Springer; 1997.
26. Younossi-Hartenstein A, Hartenstein V. Pattern, time of birth, and morphogenesis of sensillum progenitors in *Drosophila*. Microsc. Res. Tech. 1997; 39:479–491. [PubMed: 9438249]
27. Brand AH, Perrimon N. Targeted gene expression as a means of altering cell fates and generating dominant phenotypes. Development. 1993; 118:401–415. [PubMed: 8223268]
28. Lin D, Goodman C. Ectopic and increased expression of Fasciclin II alters motoneuron growth cone guidance. Neuron. 1994; 13:507–523. [PubMed: 7917288]

29. Tracey WD, Wilson RI, Laurent G, Benzer S. painless, a *Drosophila*-gene essential for nociception. Cell. 2003; 113:261–273. [PubMed: 12705873]
30. Hassan BA, Bermingham NA, He Y, Sun Y, Jan YN, Zoghbi HY, Bellen HJ. atonal regulates neurite arborization but does not act as a proneural gene in the *Dro sophila* brain. Neuron. 2000; 25:549–561. [PubMed: 10774724]
31. Bashaw GJ, Kidd T, Murray D, Pawson T, Goodman CS. Repulsive axon guidance: Abelson and Enabled play opposing roles downstream of the roundabout receptor. Cell. 2000; 101:703–715. [PubMed: 10892742]
32. Fan X, Labrador JP, Hing H, Bashaw GJ. Slit stimulation recruits Dock and Pak to the roundabout receptor and increases Rac activity to regulate axon repulsion at the CNS midline. Neuron. 2003; 40:113–127. [PubMed: 14527437]
33. Inbal A, Levanon D, Salzberg A. Multiple roles for u-turn/ventral veinless in the development of *Drosophila* PNS. Development. 2003; 130:2467–2478. [PubMed: 12702660]
34. Salzberg A, D'Evelyn D, Schulze KL, Lee JK, Strumpf D, Tsai L, Bellen HJ. Mutations affecting the pattern of the PNS in *Drosophila* reveal novel aspects of neuronal development. Neuron. 1994; 13:269–287. [PubMed: 8060613]
35. Jarman AP, Grau Y, Jan LY, Jan YN. atonal is a proneural gene that directs chordotonal organ formation in the *Drosophila* peripheral nervous system. Cell. 1993; 73:1307–1321. [PubMed: 8324823]
36. Halfon MS, Gisselbrecht S, Lu J, Estrada B, Keshishian H, Michelson AM. New fluorescent protein reporters for use with the *Drosophila* Gal4 expression system and for vital detection of balancer chromosomes. Genesis. 2002; 34:135–138. [PubMed: 12324968]
37. Kolodziej PA, Jan LY, Jan YN. Mutations that affect the length, fasciculation, or ventral orientation of specific sensory axons in the *Drosophila* embryo. Neuron. 1995; 15:273–286. [PubMed: 7646885]
38. Zlatic M, Landgraf M, Bate M. Genetic specification of axonal rbors. atonal regulates robo3 to position terminal branches in the *Drosophila* nervous system. Neuron. 2003; 37:41–51. [PubMed: 12526771]
39. Martin-Bermudo MD, Dunin-Borkowski OM, Brown NH. Specificity of PS integrin function during embryogenesis resides in the alpha subunit extracellular domain. EMBO J. 1997; 16:4184–4193. [PubMed: 9250662]
40. Kurant E, Pai CY, Sharf R, Halachmi N, Sun YH, Salzberg A. Dorsotonals/homothorax, the *Drosophila* homologue of meis1, interacts with extradenticle in patterning of the embryonic PNS. Development. 1998; 125:1037–1048. [PubMed: 9463350]
41. Heuer JG, Kaufman TC. Homeotic genes have specific functional roles in the establishment of the *Drosophila* embryonic peripheral nervous system. Development. 1992; 115:35–47. [PubMed: 1353440]
42. Keleman K, Rajagopalan S, Cleppien D, Teis D, Paiha K, Huber LA, Technau GM, Dickson BJ. Comm sorts robo to control axon guidance at the *Drosophila* midline. Cell. 2002; 770:415–427. [PubMed: 12202032]
43. Wu W, Wong K, Chen J, Jiang Z, Dupuis S, Wu JY, Rao Y. Directional guidance of neuronal migration in the olfactory system by the protein Slit. Nature. 1999; 400:331–336. [PubMed: 10432110]
44. Brose K, Tessier-Lavigne M. Slit proteins: key regulators of axon guidance, axonal branching, and cell migration. Curr. Opin. Neurobiol. 2000; 10:95–102. [PubMed: 10679444]
45. Hu H. Chemorepulsion of neuronal migration by Slit2 in the developing mammalian forebrain. Neuron. 1999; 23:703–711. [PubMed: 10482237]
46. Chen, J-h; Wen, L.; Dupuis, S.; Wu, JY.; Rao, Y. The N-terminal leucine-rich regions in Slit are sufficient to repel olfactory bulb axons and subventricular zone neurons. J. Neurosci. 2001; 21:1548–1556. [PubMed: 11222645]
47. Mason HA, Ito S, Corfas G. Extracellular signals that regulate the tangential migration of olfactory bulb neuronal precursors: inducers, inhibitors, and repellents. J. Neurosci. 2001; 21:7654–7663. [PubMed: 11567055]

48. Bier E, Jan LY, Jan YN. rhomboid, a gene re quired for dorsoventral axis establishment and peripheral nervous system development in *Drosophila melanogaster*. Genes Dev. 1990; 4:190–203. [PubMed: 2110920]

49. Hivert B, Liu Z, Chuang C-Y, Doherty P, Sundaresan V. Robo1 and Robo2 are homophilic binding molecules that promote axonal growth. Mol. Cell. Neurosci. 2002; 21:534–545. [PubMed: 12504588]

50. Rhee J, Mahfooz NS, Arregui C, Lilien J, Balsamo J, VanBerkum MF. Activation of the repulsive receptor Roundabout inhibits N-cadherin-mediated cell adhesion. Nat. Cell. Biol. 2002; 4:798–805. [PubMed: 12360290]

51. Long H, Sabatier C, Ma L, Plump A, Yuan W, Ornitz DM, Tamada A, Murakami F, Goodman CS, Tessier-Lavigne M. Conserved roles for Slit and Robo proteins in midline commissural axon guidance. Neuron. 2004; 42:213–223. [PubMed: 15091338]

52. Mann RS, Chan SK. Extra specificity from extra-denticle: the partnership between HOXand PBX/EXD homeodomain proteins. Trends Genet. 1996; 12:258–262. [PubMed: 8763497]

53. Ryoo HD, Marty T, Casares F, Affolter M, Mann RS. Regulation of Hox target genes by a DNA bound Homothorax/Hox/Extradenticle complex. Development. 1999; 126:5137–5148. [PubMed: 10529430]

54. Pai CY, Kuo TS, Jaw TJ, Kurant E, Chen CT, Bessarab DA, Salzberg A, Sun YH. The Homothorax homeoprotein activates the nuclear localization of another homeoprotein, extradenticle, and suppresses eye development in *Dro sophila*. Genes Dev. 1998; 12:435–446. [PubMed: 9450936]

55. Fujita SC, Zipursky SL, Benzer S, Ferrus A, Shotwell SL. Monoclonal antibodies against the *Drosophila* nervous system. Proc. Natl. Acad. Sci. USA. 1982; 79:7929–7933. [PubMed: 6818557]

56. Schmid A, Chiba A, Doe C. Clonal analysis of *Drosophila* embryonic neuroblasts: neural cell types, axon projections and muscle targets. Development. 1999; 126:4653–4689. [PubMed: 10518486]

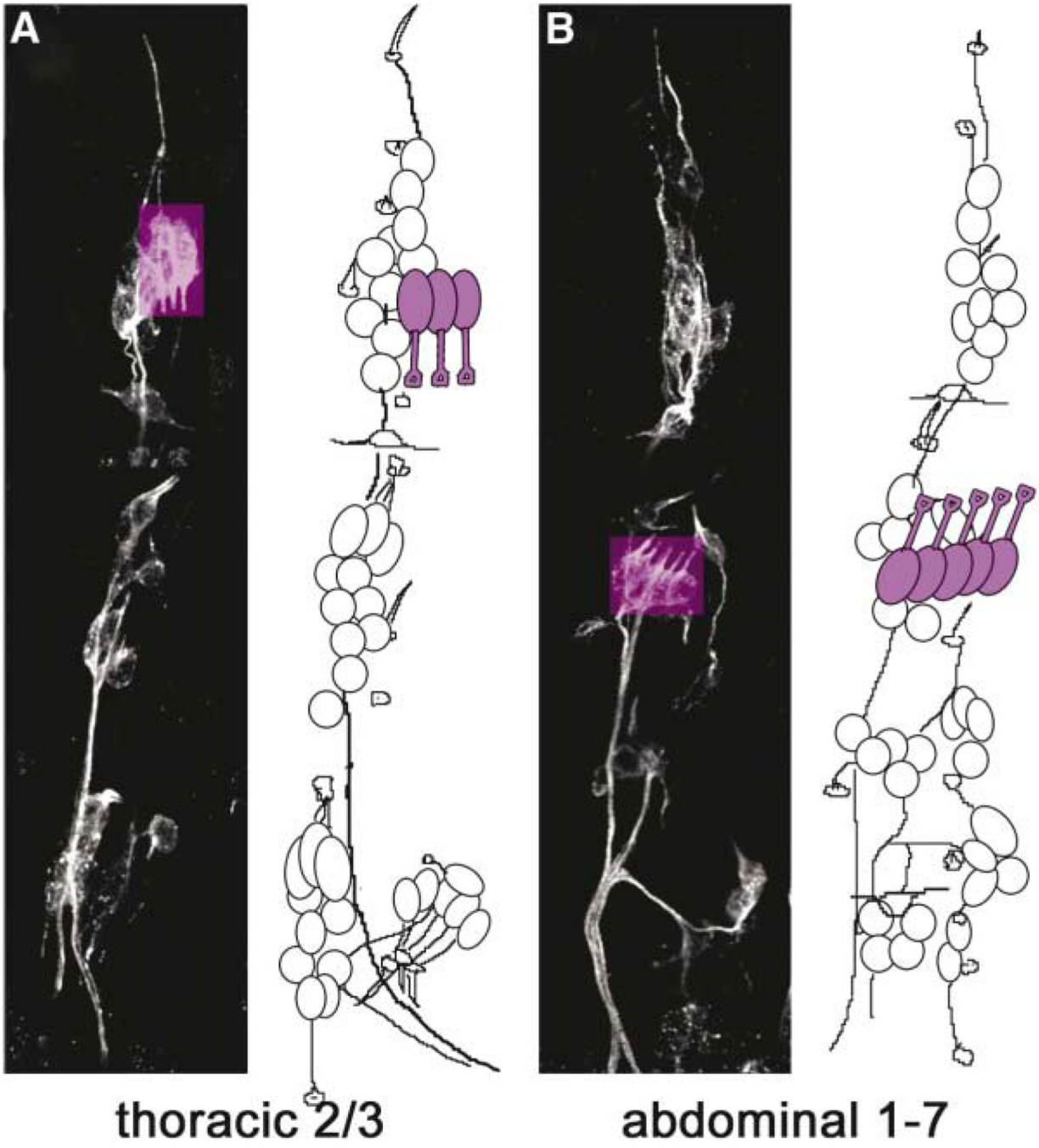


**Figure 1. Sense Organs in a Late Embryo**

Thoracic (A) and abdominal (B) segments in the epidermis of an embryo stained with mAb22C10 to label all sensory neurons. Confocal projections are shown on the left in each panel, and schematic drawings on the right show locations of cell bodies. Chordotonal organ neurons are highlighted in purple. The clusters of three thoracic Cho neurons in T2 and T3 (dCh3) are located dorsally and their dendrites point downward, whereas clusters of five Cho neurons in abdominal segments 1–7 (lCh5) are located laterally, and their dendrites point upward. Dorsal is up and anterior is left in all panels. Drawings adapted with permission from Campos-Ortega and Hartenstein [25].

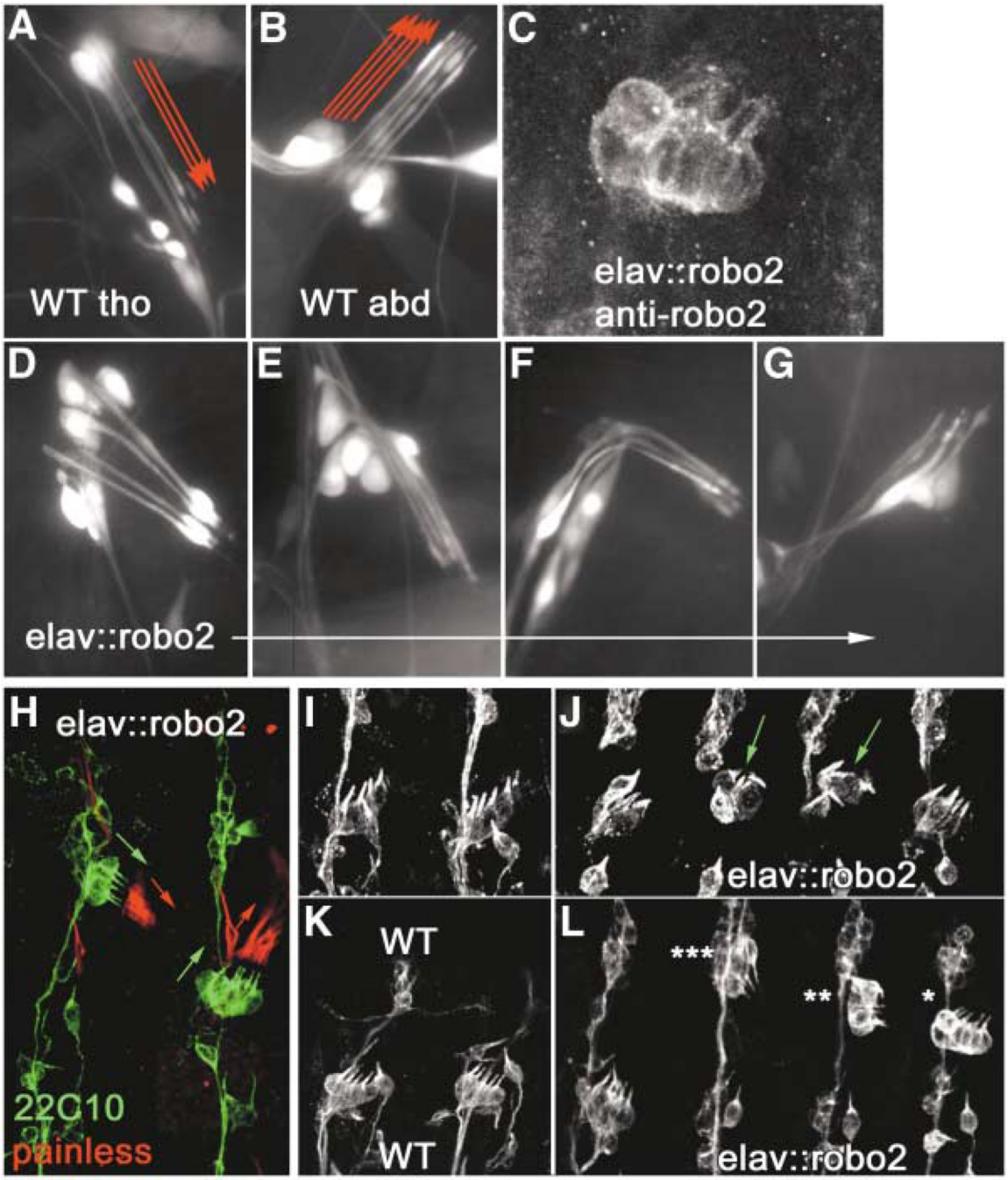


**Figure 2. Overexpression of Robo2 in Chordotonal Neurons Transforms Abdominal Organs to a Thoracic Morphology and Position**

(A and B) Wild-type third instar larval thoracic dCh3 and abdominal lCh5 neuron clusters, respectively, expressing GFP from the *elav* driver. Note the downward-pointing (ventral) orientation of thoracic dCh3 dendrites and the upward-pointing (dorsal) orientation of abdominal lCh5 dendrites (red arrows).

(C) *elav::robo2* embryonic lCh5 stained for Robo2.

(D–G) Larval abdominal lCh5s transformed to varying degrees toward the thoracic morphology, with dendrites either pointing downward as in a wild-type thoracic dCh3 (D and E) or twisted in an intermediate position (F) or simply stunted (G).

(H) Sense organs of an *elav::robo2* embryo labeled with mAb 22C10 (green) and anti-Painless (red) to show orientation of neurons in two abdominal lCh5s (green arrows), one transformed toward thoracic type (left) and one not (right). Anti-Painless labels the Cho cap cells (red arrows), which do not express Robo2, but follow the orientation of the Cho neurons that do.
(I and K) Wild-type abdominal segments at late stage 14 and stage 15, respectively, stained with 22C10 to show orientation of Cho neurons.
(J) *elav::robo2* abdominal lCh5s at stage 14, the earliest stage at which transformed lCh5s (green arrows) can be unambiguously recognized in a fixed preparation.
(L) *elav::robo2* abdominal lCh5s at stage 15, showing various classifications of transformation: complete (triple star), partial (double star), and shifted (single star).

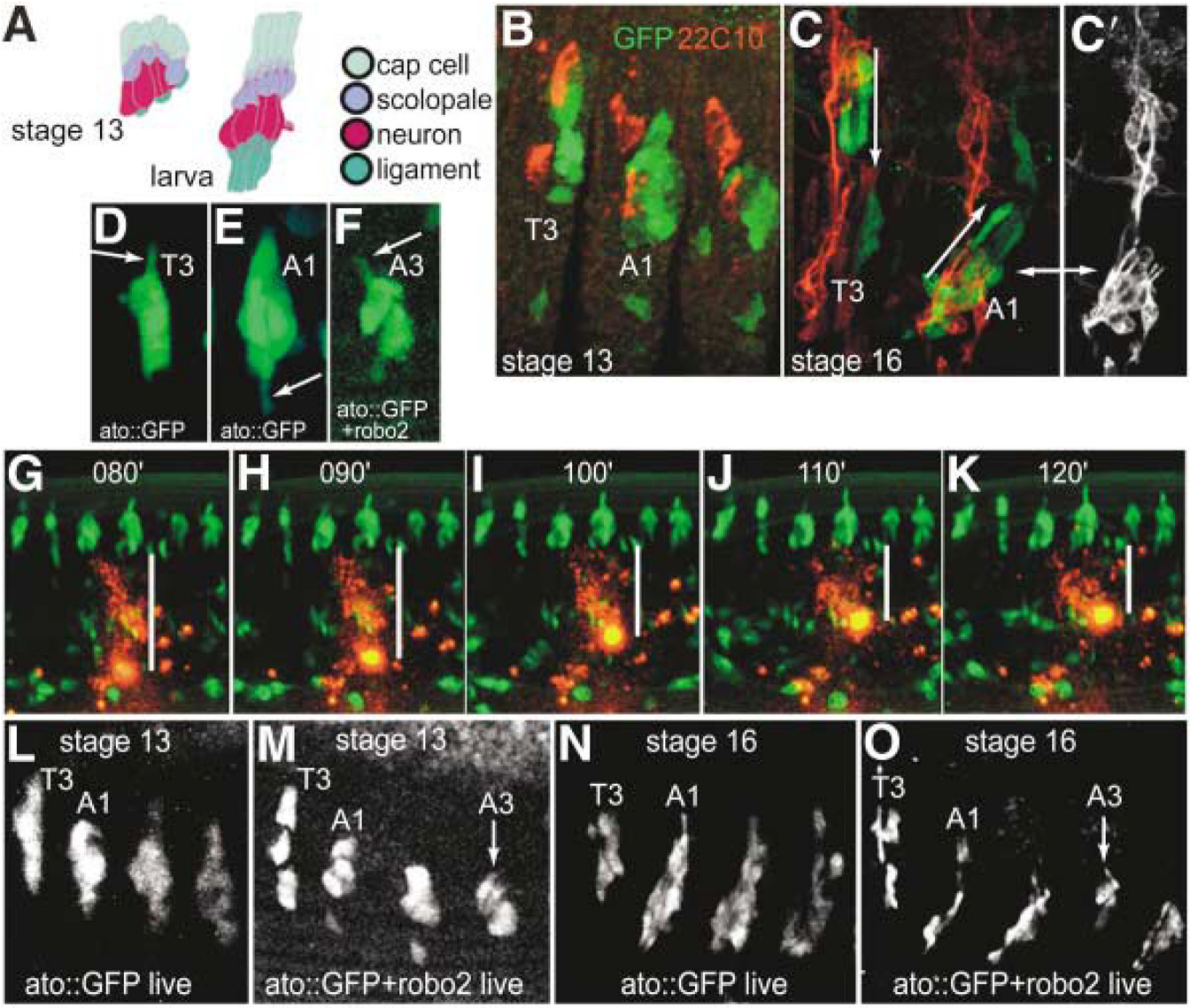


**Figure 3. Live Observation of Migrating Chordotonal Organ Precursors**

(A) Schematic representations of abdominal chordotonal organs in a stage 13 embryo versus the larva. Each organ, which is present in abdominal segments as clusters of five (shown), consists of a cap cell, which anchors the organ to the epidermis at the dorsal tip, a scolopale, which ensheathes the dendrite, a neuron, which possesses a prominent dendrite, and a ligament cell, which anchors the organ at its ventral side. This arrangement is reversed in thoracic segments, so that the cap cells point ventrally rather than dorsally (adapted with permission from Campos-Ortega and Hartenstein[25], Figure 9.2).

(B) A stage 13 embryo expressing *atonal*-GAL4 driven GFP in all Cho precursors (green) and labeled for 22C10 (red), which labels the neurons of all sense organs. T3, third thoracic segment; A1, first abdominal segment in all panels.

(C) A stage 16 embryo labeled in the same manner, showing further refinement of GFP expression such that the orientation of Cho organs is apparent. Cho organs have dendrites pointing ventrally in thoracic segments and dorsally in abdominal segments (arrows). (C′) 22C10 expression alone shows the location of neurons, by which the orientation of the organ

can easily be recognized, in relation to the GFP pattern (double arrow points to the same lateral Cho cluster in each panel).

(D–F) Stills from time-lapse series of developing Cho organs in a control embryo (*ato*::GFP), and an embryo expressing both GFP and Robo2 in Cho organs (see Movies 1 and 2 online). Here, at early stage 14, as Cho organs begin to actively migrate, processes (arrows) can be seen protruding from either the dorsal side in a thoracic segment (D) or the ventral side in an abdominal segment (E) of a normal embryo. In the embryo expressing Robo2 in Cho precursors (F), a process extends from the dorsal side (arrow) of an abdominal Cho precursor, similar to that seen in a thoracic segment.

(G–K) Still images from time-lapse movie of a wild-type (*ato*::GFP) embryo injected with a spot of DiI to show movement of abdominal Chos relative to the surrounding epidermis. White bars show that the distance from the ventral-most extent of the Cho organs to the center of the DiI spot diminished over time (numbers represent frames of the movie, taken every 1 min).

(L–O) Still images from time-lapse movies of developing control Chos (*ato*::GFP) versus Robo2-overexpressing Chos (*ato*::GFP+ robo2) at stages 13 and 16, showing one thoracic segment and three abdominal segments in each panel. Note that by stage 16, the final orientation of the organ is evident, with abdominal Chos positioned more ventrally and oriented oppositely to thoracic Chos (compare [N] to [C]). They reach this position from more equivalent dorsoventral positions at stages 12 and 13 (as in [L] and [M]) by a ventral migration (G–K, and see Movie 1). Note that the A3 lCh5 in the Robo2-overexpressing embryo (O) has failed to migrate and remained in a thoracic position (arrow). The slight dorsal displacement of anterior (T3 and A1) relative to posterior (A2 and A3) Chos at stage 13 (L and M) is caused by the curvature of the germ-band during gastrulation. Less GFP is evident in the *ato*::GFP+ robo2 shown in (F), (M), and (O) because it contains only one copy of UAS-GFP.

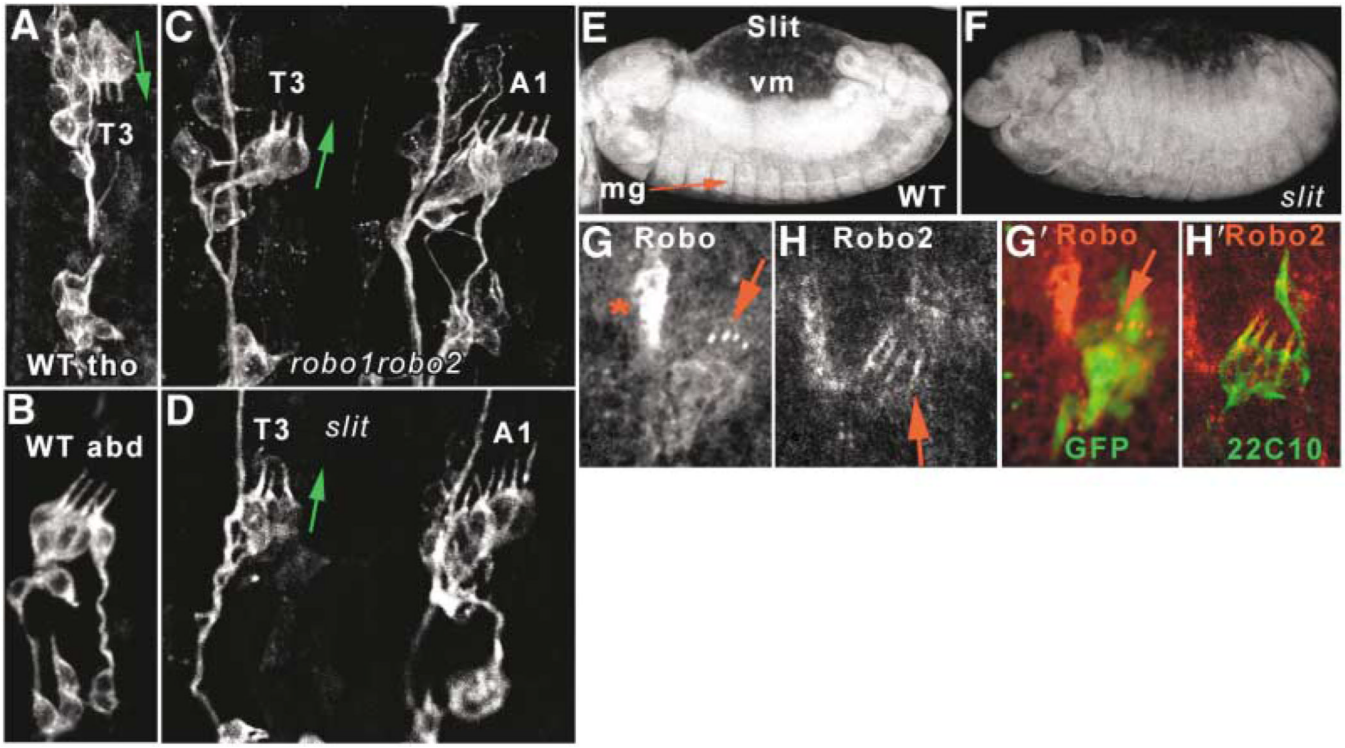


**Figure 4. *robo, robo2* and *slit* Mutations Cause Thoracic-to-Abdominal Transformations of Chordotonal Organs**

(A–D) Cho organs in stage 16 embryos visualized with mAb 22C10. (A) Wild-type thoracic dCh3 dorsally positioned and with dendrites pointing downward (green arrow), versus (B) wild-type lCh5 with dendrites pointing upward. (C) *robo, robo2* double mutant; (D) *slit* mutant. Both have thoracic dCh3s positioned laterally with dendrites pointing upward (green arrow), adjacent to similarly oriented A1 lCh5 organs.

(E and F) Slit expression in a stage 13 wild-type embryo (E), showing strong expression in midline glia (mg) and in visceral mesoderm (vm); this expression is absent in a *slit* mutant embryo of the same age (F), imaged with identical settings. Slit is not detected in Cho organs.

(G and H) Expression of Robo and Robo2 proteins in wild-type stage 15 Cho neurons. Robo is expressed weakly in the cell bodies and strongly in the dendrite tips, while Robo2 is detected mainly in the dendrites (red arrows). Red star denotes muscle attachment site Robo expression. (G′) and (H′) show colocalization with *elav*::GFP (G′) or 22C10 (H′) to show location of Cho neurons.

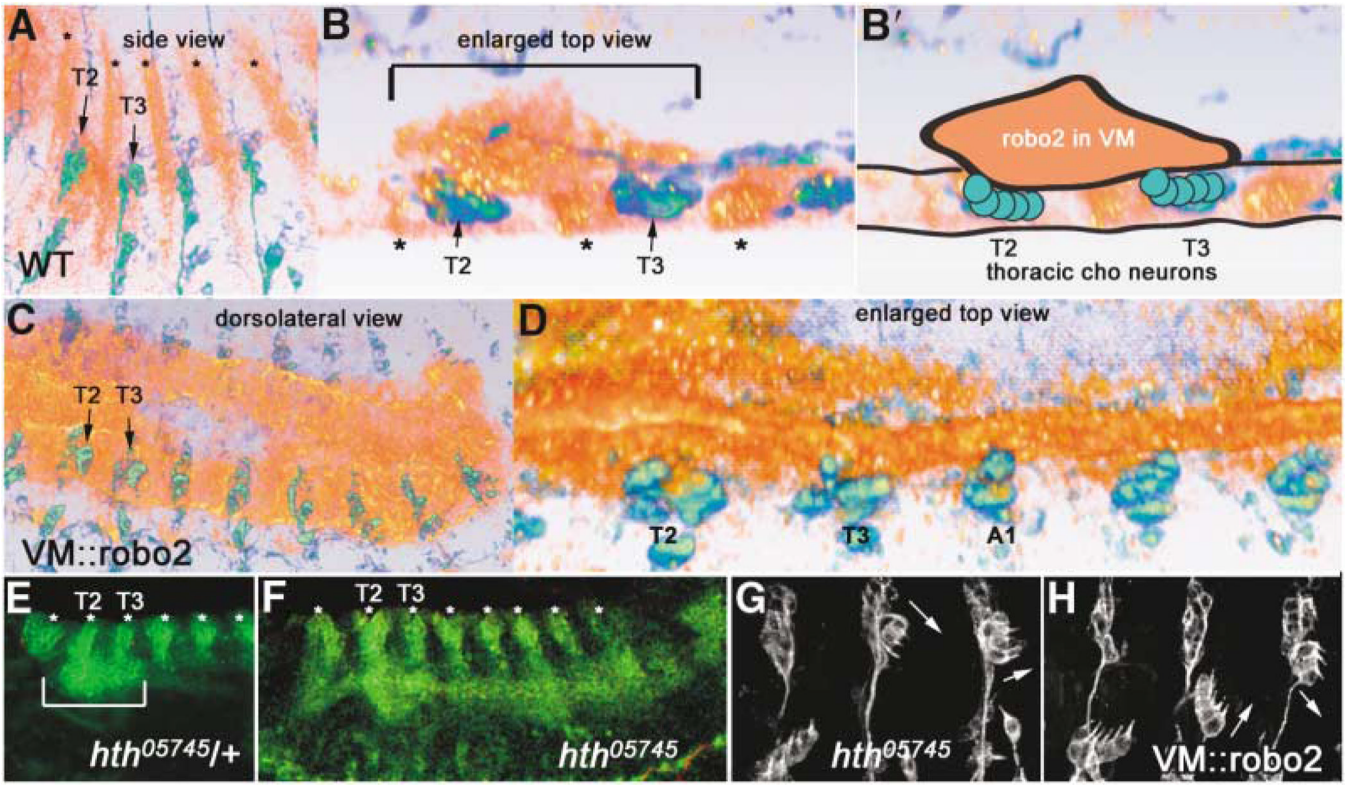


**Figure 5. Robo2 Is Expressed in Thoracic Visceral Mesoderm Apposed to Thoracic Chordotonal Neurons, in a Domain Defined by Homeotic Gene Eepression**

(A and B) 22C10 (green/blue) and Robo2 (orange/red) expression in a wild-type stage 14 embryo, shown by volume rendering of a con-focal stack (Amira software). Ectodermal stripes of Robo2 expression are denoted by asterisks.

(A) Side view shows anterior-posterior and dorsoventral extent of Robo2 expression in VM in T2 and T3.

(B) Spatial proximity of the Robo2 VM expression to thoracic Chos can be better visualizedin an enlarged top view (horizontal section)through the same confocal stack, where the thoracic VM Robo2 expression domain is bracketed above the dCh3s in T2 and T3. Interior of the embryo is up. An animated view of the Robo2 expression domains compared to 22C10 can be seen in Movie 3 online.

(B′) Schematic representation of the image in (B), outlining the clump of Robo2 expression in the VM (orange) apposed to thoracic Cho neurons in T2 and T3 (green circles).

(C and D) Ectopic expression of Robo2 with a VM GAL4 driver, showing full posterior extent of robo2 expression at similar stage (C; compare to A) and an enlarged top view (D; compare to B).

(E and F) *homothorax* mutant embryos at stage 13 (F) have an expanded Robo2 expression domain in the VM (green continuous horizontal stripe that appears to connect the bottoms of the vertical ectodermal Robo2 stripes [asterisks]); compare this pattern to the control *(hth/+)* embryo (E), whose Robo2 VM expression domain is only in T2 and T3 (bracket).

(H) Driving Robo2 in the abdominal VM transforms Cho organs; the transformed morphologies are identical to those seen when Robo2 is driven in neurons or Cho organs (Figure 2).

(G) A similar phenotype is observed in an *hth* mutant. Transformations of abdominal lCh5s are noted by arrows. All embryos are oriented with anterior to the left and dorsal up unless otherwise noted. (E) and (F) are slightly ventrolateral views.

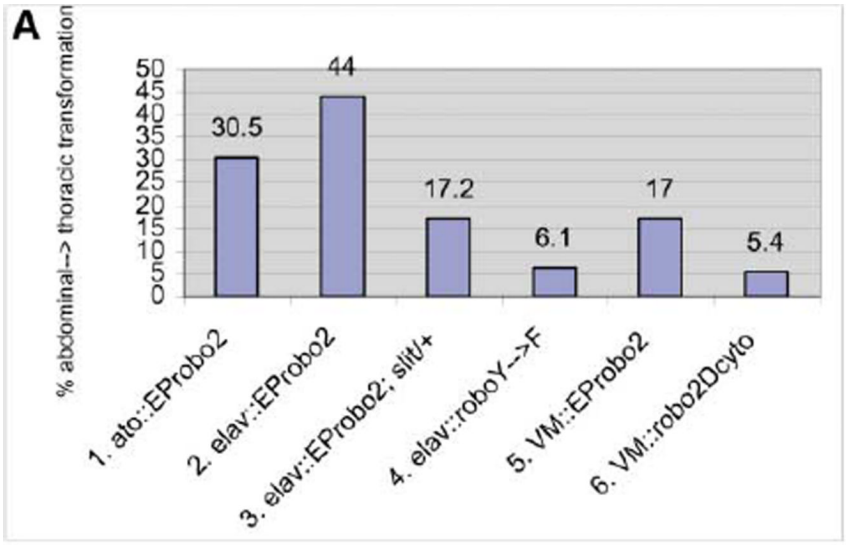


Gain-of-function Cho transformation rates

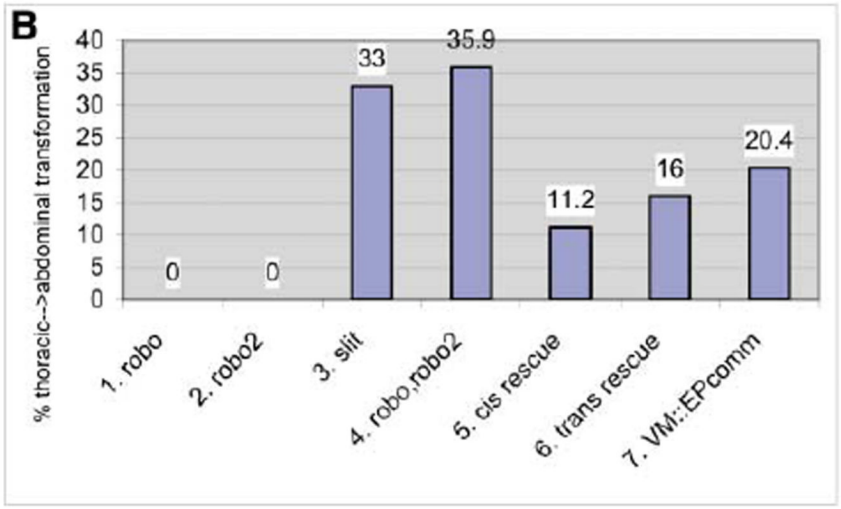


Loss-of-function Cho transformation rates and rescue

**Figure 6. Summary of Gain-of-Function and Loss-of-Function Cho Organ Phenotypes**

(A) Percentages of abdominal→thoracic transformation (migration failure) produced by overexpression of Robo family proteins. Over-expression of Robo2 in Cho neurons (columns 1 and 2) or in the VM (5) produces transformation; this is attenuated by removal of one copy of *slit* (3). Hyperactivated Robo (4) and Robo2 lacking the cytoplasmic domain (robo2Dcyto; 6) can also transform at a low frequency.

(B) Percentages of thoracic→abdominal transformation (ectopic migration) produced by loss of function of Robos and Slit. *slit* (3) and *robo, robo2* mutants (4) display transformation, but *robo* (1) and *robo2* (2) single mutants do not. The phenotypes of *robo, robo2* mutants are partially rescued by either *cis* (neuronal; *elav::UAS-robo2;* 5) or *trans*

(mesodermal; *48Y::UASrobo2;* 6) expression of a *robo2*$^{myc}$ transgene in a *robo, robo2* background. Expression of Comm in the VM, which would downregulate all robos in that tissue *(48Y-GAL4 × EP-Comm)*, induces transformation (7).

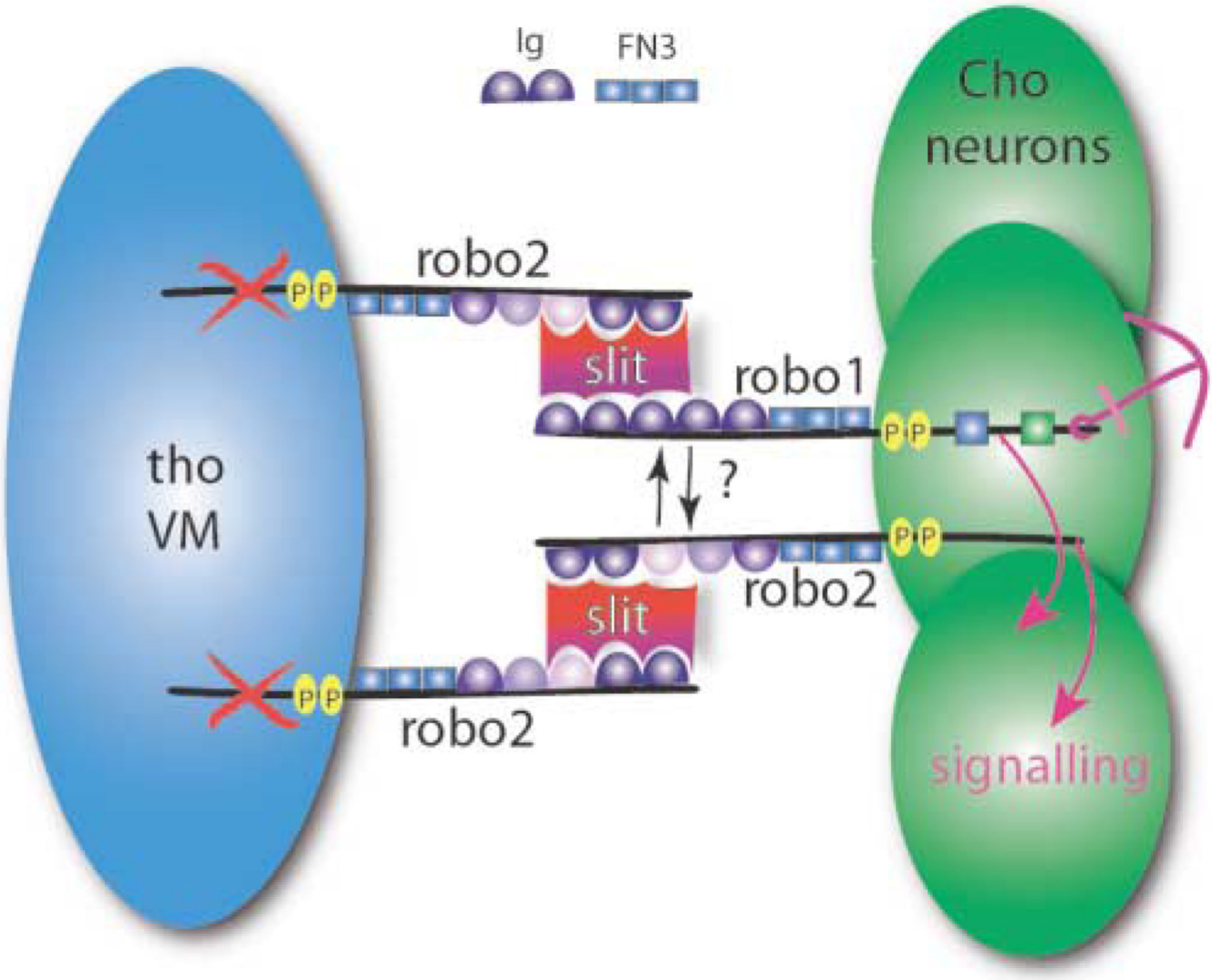


**Figure 7. Slit Sandwich Model for Signaling between Visceral Mesoderm and Chordotonal Neurons**

Robo and Robo2 are expressed on Cho neurons (green), where both contribute to signaling (pink arrows). Signaling by Robo and Robo2 is triggered by binding of Slit (red/purple shape) to Robo2 on thoracic visceral mesoderm (tho VM; blue); this "presents" Slit in *trans* to Robo and Robo2 on Cho neurons. The ×s on tho VM indicate that the Robo2 cytoplasmic domain is not essential for signaling in *trans.* FN3 and Ig, domains of Robo/Robo2; P, CC0, CC1 motifs (can be phosphorylated); green and blue boxes, Robo CC2 and CC3 motifs. Anchor indicates that the consequence of signaling is the prevention of migration.

## Table 1

Gain-of-Function Cho Organ Phenotypes

| Driver | Gene/Construct | % Partial/Complete Transformation[a] | % Total Defects[b] | Number/Type of Hemisegments[c] |
|---|---|---|---|---|
| Elav | *EP-robo2* | 44 | 58.4 | 457 abd |
| Atonal | *EP-robo2* | 30.5 | 40 | 151 abd |
| Elav | *UAS-robo2*[d] | 21 | 41 | 56 abd |
| Elav | *UAS-robo*$^{Y\rightarrow F}$ | 6.1 | 8.7 | 196 abd |
| Elav | *UAS-robo*$^{icc2cc3}$ | 0 | 0 | 119 abd |
| Elav | *UAS-robo3*[d] | 0 | 0 | 364 abd |
| Elav | *EP-robo2 (25°C)* | 32 | 58 | 262 abd |
| Elav | *EP-robo2; +/slit*$^{-}$ *(25°C)* | 17.2 | 32.6 | 319 abd |
| Elav | *EP-robo2, robo*$^{Z2130}$ | 36.4 | 49.4 | 324 abd |
| VM | *EP-robo2* | 17 | 41 | 247 abd |
| | | 0 | 1.5 | 68 tho |
| VM | *UAS-robo3*[d] | 0 | 0 | 70 abd |
| VM | *UAS-robo2-Δcyto*[d] | 5.4 | 14.2 | 742 abd |
| | | 9 | 10.8 | 212 tho |
| VM | *UAS-robo*$^{Y\rightarrow F}$ | 0.2 | 0.7 | 406 abd |
| | | 0 | 0.9 | 114 tho |

All experiments were performed at 29°C unless specified otherwise.

Abbreviations: abd, abdominal segments; tho, thoracic segments.

[a] Similar to triple or double asterisked examples shown in Figure 2J.

[b] Similar to any of the defects shown in Figure 2J.

[c] Thoracic segments were unaffected unless specified otherwise.

[d] *robo2* and *robo3* transgenes are myc-tagged.

**Table 2**

Loss-of-Function Cho Organ Phenotypes

| Genotype | Rescue | % Tho→Abd Transformation[a] | Number of Thoracic Hemisegments |
|---|---|---|---|
| *robo*$^{Z2130}$ | | 0 | 71 tho |
| *robo2* $^{ex135}$ | | 0 | 100 tho |
| *slit*$^{2}$ | | 33 | 108 tho |
| *robo*$^{GP285}$, *robo2* $^{ex135}$ | | 35.9 | 75 tho |
| *robo*$^{Z2130}$, *robo2* $^{ex135}$ | *elav::robo2-myc (cis)* | 11.2 | 107 tho |
| *robo*$^{Z2130}$, *robo2* $^{ex135}$ | *VM::robo2-myc (trans)* | 16 | 69 tho |
| *VM::EP-commissureless* | | 20.4 | 211 tho |

[a]Similar to thoracic segments shown in Figures 4C and 4D.